Numerical Analysis of the Source of Excessive Na^+ and Cl^- Species in Flowback Water from Hydraulically Fractured Shale Formations

Maxian B. Seales, The Pennsylvania State University; **Robert Dilmore,** National Energy Technology Laboratory; **Turgay Ertekin**, and **John Yilin Wang**, The Pennsylvania State University

Summary

Fracture fluid comprises fresh water, proppant, and a small percentage of other additives, which support the hydraulic fracturing process. Excluding situations in which flowback water is recycled and reused, total dissolve solids in fracture fluid is limited to the fluid additives, such as potassium chloride (1-7 weight percent KCL), which is used as a clay stabilizer to minimize clay swelling, and clay particle migration. However, the composition of recovered fluid, especially as it relates to the total dissolve solids (TDS), is always substantially different than the injected fracture fluid.

The ability to predict flowback water volume and composition is useful when planning for the management or reuse of this aqueous byproduct stream. In this work, an ion transport and halite dissolution model was coupled with a fully implicit, dual porosity, numerical simulator, to study the source of the excess solutes in flowback water, and to predict the concentration of both Na^+ and Cl^- species seen in recovered water. The results showed that mixing alone, between the injected fracture fluid and concentrated in situ formation brine, could not account for the substantial rise in TDS seen in flowback water. Instead, the results proved that halite dissolution is a major contributor to the change in TDS seen in fracture fluid during injection and recovery. Halite dissolution can account for as much as 81% of Cl^- and 86.5% of Na^+ species seen in 90-day flowback water; mixing, between the injected fracture fluid and in situ concentrated brine, accounts for approximately 19% Cl^- and 13% Na^+.

Keywords: Shale gas, flowback water, total dissolve solids

Introduction

Horizontal wells combined with successful multi-stage hydraulic fracture (HF) treatments are currently the industry accepted standard for effectively stimulating, and enabling economic development of natural gas resources organic-rich shale formations. All hydraulic fracture (HF) treatments require a post-stimulation flow period (cleanup) that returns the fracture fluid to the surface, and prepares the formation stimulated reservoir volume for long-term production. However the reservoir typically retains a significant percentage of the injected fluid that is a function of the formation geology, fracture treatment design, and subsequent operating procedures. Fracture fluid recovery in Marcellus shale ranges from 2 to 26%, with an average recovery of 6.6% (Zhou, 2015) There is no consensus explanation for such a low volumetric recovery. Some researchers have attributed the volume loss to fluid being retained in nonconductive portions of the stimulated reservoir volume, and in spaces that were previously occupied by salts that were dissolved by the fracture fluid (Gdanski, Weaver et al. 2007; Blauch, Myers et al. 2009). Yet, others point to fluid imbibition into the rock matrix, initiated and supported by high capillary forces.

For a 5 million gallon treatment, flowback water in Marcellus shale, on average, can be expected to be in the range of 450,000 to 750,000 gallons. This aqueous byproduct stream typically contains proppants, dissolved salts and other minerals. Chemical analysis performed on flowback water shows that the TDS can reach concentrations that are 10 to 20 times greater than those present in the injected fluid (Hayes and Severin 2012). Haluszczak, Rose et al (2013) presented data, showing TDS concentrations in flowback water as high as 197,000mg/L, with chloride levels as high as 151,000 mg/L (Haluszczak, Rose et al. 2013). Stepan, Shockey et al (2010), in their analysis of the feasibility of recycling flowback water in Bakken Shale, noted TDS concentrations in the region of 200,000 ppm. Laboratory measurements performed on the flowback water from 12 hydraulically fractured Marcellus shale wells shows that Na^+ and Cl^- species account for 87% to 90% of the TDS, and other species such as K^+, Ca^{2+} and Mg^{2+} etc. account for the remaining 10 to 13% (Hayes and Severin, 2012). These TDS concentrations are several times higher than that of seawater (35,000 mg/L). Current knowledge suggests that the high TDS in flowback water is the direct result of salt dissolution in the formation. However, some researchers believe that the extra solute added to the HF fluid, and recovered during flowback, is primarily the result of mixing between injected fluid and concentrated in situ brines.

Management of flowback and produced water is important, both to maximize water reuse and minimize freshwater resource utilization, and to ensure that those water resources are not contaminated as a result of mismanagement of those byproduct waters. However, publicly owned wastewater treatment works (POTWS), and most central water treatment (CWT) facilities cannot process this wastewater stream to an acceptable level that will permit disposal into surface streams (Puder and Veil 2006). Treatment requires specialize processes such as crystallization, thermal distillation, electrodialysis, reverse osmosis, forward osmosis and/or ion exchange, which are expensive and energy intensive. Therefore such processes are not typically found at

POTWs or CWTs. Operators are now assessing the feasibility of onsite recycling as a means of reducing fresh water consumption and reducing wastewater volumes. Advancements in technology have lead to the development of mobile onsite treatment plants that can be relocated from site to site, or incorporated into onsite water recycling systems (Paugh 2008; Horn 2009; Stepan, Shockey et al. 2010; Shafer 2011). Ultimately, designing and implementing the most efficient flowback water management scheme will require an ability to predict the volume and composition of flowback and produced water that will be recovered (Yang, 2015).

There is variability in every formation, even among wells/fields in the same shale formation. For this reason, one cannot assume, neither can one plan and design water treatment facilities, on the assumption that the composition of flowback water from each field, across different formations, is identical. Correct flowback water composition (TDS) is an essential input needed to determine the most cost effective and efficient method for treating this wastewater source. The model presented in this paper is intended to start the process of closing this gap in knowledge by enhancing our ability to more accurately predict the composition of flowback water from hydraulically fractured formations, thus allowing for better planning and frontend designs for flowback water treatment, reuse and/or disposal. To more accurately predict flowback water composition, one must first capture the correct physical and chemical processes at work in the formation that controls this composition. Determining the source of the large amounts of dissolve species recovered in flowback water is one of the first steps needed to accurately predict the ionic composition of this wastewater stream. Therefore, in so doing, the manuscript also provides additional evidence to the academic debate on the source of the excess Na^+ and Cl^- species captured by the injected fluid. Is the source of these ions the insitu concentrated brines, or are these ions entering the flowback water stream through the dissolution of salts such as Halite? Ultimately, it is our hope that this model can aid the petroleum industry in planning the treatment, reuse, and final disposal of flowback and produced water. Additional, we think it can be used as a management tool by government agencies who are interested in accurately predicting the TDS in flowback water for public and environmental health reasons.

Though compositional modeling has seen significant research efforts in petroleum engineering, work on flowback water characterization through compositional models is quite limited. There has been only one published research on flowback water characterization through compositional models within the last decade. Gdanski and Weaver presented a model that simulated the change in the ionic concentration of injected fluid in a tight gas formation as a function of time and volume of recovered fluid. This work was intended to determine the fraction of recovered water that was actually injected fluid and that which was insitu formation brine. This was achieved through comparisons among the simulated flowback water composition, the injected fluid composition and the formation brine composition (Gdanski, Weaver et al. 2007). Apart from this research context that addresses flowback water ionic composition from hydraulically fractured formations, one of the more widely cited work on compositional modeling is that by Liu and Ortoleva 1996. These researchers presented a methodology to develop a multipurpose geochemical simulator, which was used to study reservoir acidization and scale formation during waterflooding (Liu and Ortoleva 1996). Other researchers investigated the reactive kinetics of enhanced oil recovery processes such as alkaline flooding (Bhuyan, Lake et al. 1990; Bazin and Labrid 1991), yet others focused on the approach needed to accurately model the change in ionic concentration with implication for ground water pollutant modeling and alkaline flooding (Bryant, Schechter et al. 1986; Walter, Frind et al. 1994).

Mineral Dissolution Kinetics

According to Stumm and Wollast (1990), mineral dissolution involves several successive elementary steps that include: (1) mass transport of dissolved reactants from bulk solution to the mineral surface, (2) adsorption of solutes, (3) interlattice transfer of reacting species, (4) surface chemical reactions, (5) detachment of reactants from the surface, and (6) mass transport into the bulk solution. The slowest of these processes is considered rate limiting, and thus controls the overall reaction rate.

Under natural conditions, the rate of mineral dissolution can typically be classified into two groups: (a) those that are controlled by the mass transfer of reactants and products in the solid phase (step 3), or (b) those that are controlled by surface chemical reactions (step 4) and the detachment of reactants from the surface (step 5). Under normal environmental conditions, dissolution rates for most minerals are too slow for the reaction to be limited by the mass transfer of reactants or products in the aqueous phase (steps 1 and step 6). However, because of their high solubility, calcareous and evaporite minerals such as halite and gypsum are thought to be exceptions to this rule - i.e., they are transport controlled dissolution mechanisms, limited by the by the mass transfer of reactants or products in the aqueous phase. Literature on the subject has identified two primary mechanisms that control these minerals dissolution rates: (1) the rate-determining step is the transport step (i.e. transport of a reactant or product through an interfacial layer on the surface of the mineral), or (2) the rate-determining step is the surface reactions and detachment of reacting species from the mineral surface. Transport controlled dissolution reactions can be described by the parabolic rate law (Stumm and Wollast 1990), given by:

$$r = \frac{dC}{dt} = k_p t^{-1/2} \quad \text{..... (1)}$$

where r is the reaction rate $[mol/m^2 s]$, C is the moles transferred per unit area $[mol/m^2]$, t is time, and k_p is the rate constant $[mol/m^2\, s^{1/2}]$.

In the event that surface reactions are slow in comparison to the transport step, the reaction rate is termed surface-controlled. In such a situation, the concentration of the solutes adjacent the reacting mineral surface will be equal to that in the bulk solution, and reaction kinetics are zero-order if steady state conditions exist on the surface(Stumm and Wollast 1990; Sparks 2003). Such a situation is seen with the dissolution of silicates and oxides; these processes follow a zero-order rate law such as that given by equation 2:

$$r = \frac{dC}{dt} = ka \qquad \text{..... (2)}$$

where r is the dissolution rate $[mol/s]$, k is the rate constant $[mol/m^2 s]$ and a $[m^2]$ is the mineral surface area.

Halite dissolution under normal environmental conditions is a transport/diffusion-controlled reaction. However, normal environmental conditions do not exist in a shale formation hydraulic fractures that are constantly abraded by high velocity fracture fluid travelling back to the wellbore during flowback. For this reason, we hypothesize that the transport of detached Na^+ and Cl^- species from the halite mass into the bulk solution is almost instantaneous. Therefore, halite dissolution in hydraulically created fractures in shale formations is not a transport-controlled process, but is likely controlled by the surface reactions. In other words: in the context of a fractured shale formation, during flowback, the rate of halite dissolution in the fractures is controlled by the rate at which NaCl is detached from the halite surface, and not by the rate at which ions diffuse across the interfacial layer into the bulk solution.

Ion Transport Numerical Model

The numerical model comprises an ion transport and halite dissolution module that is sequentially coupled to a fully implicit, dual porosity, finite difference simulator (**Fig. 1**). Development of the fully implicit, dual porosity simulator has been presented in other work by the authors, and will not be repeated here. The ion transport equations that are solved each time step for the matrix and fracture domains are presented as **Eq. 3** and **Eq. 4**; both are presented in 1-Dimension for clarity. Specific details on the development of these equations can be found in other works by the authors (Seales, Wang et al 2015). The halite dissolution module is coupled to the ion transport module by treating the dissolved Na^+ and Cl^- species as additional source terms in the ion transport equations. In developing the halite dissolution model, it was assumed that if halite is present in the shale matrix, the only possible source of these salt must be from concentrated brine that existed in the pore spaces of the rock matrix. Working with this premise, the model assumes that any halite present in the shale matrix must be accumulate on the surfaces of the pore spaces inside the rock matrix. However, halite that may be found in micro fractures were not considered because the occurrence, size and distribution of these fractures is not consistent. Therefore, the mass of halite that may be found in such fractures, in say a cubic foot of the shale matrix, will be inconsistent and not readily predictable. Further details on the model development, model inputs such as relative permeability and capillary pressure curves, and the dual porosity model validation, can be found in other works by the authors (Seales, Wang et al 2015; Seales, Dilmore et al 2015).

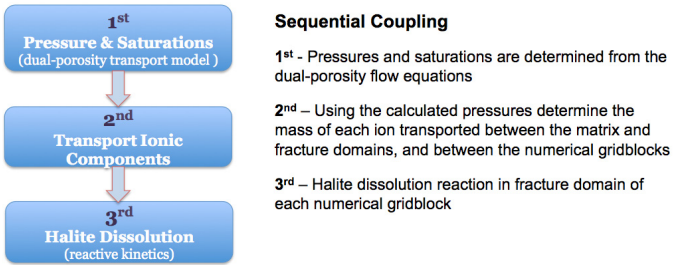

Figure 1: Numerical model illustration

At this point, it is important to note that the model captures the change in dissolve species concentration in the simulated reservoir by tracking the mass of each dissolve species, and the mass of water entering and leaving all numerical gridblocks. Similarly, the mass of flowback water and the mass of each dissolve species in this water is captured. This approach allows the concentrations to be determined in molality (mass/mass) instead of molarity (mass/volume), which avoids the problems associated with changes in volume caused by differences in pressure across each numerical gridblock, and between subsurface and surface conditions. However, for the purpose of comparison to field data, which is reported in grams of solute per volume of solvent (g/L), simulated concentration are converted from mass of solute per mass of solvent to mass of solute per volume of solvent (g/L) and reported as such in this manuscript.

Ion Transport Equation for the Fracture Domain

$$\frac{\partial}{\partial x}\left[T_{Fx}\left(\frac{\partial p}{\partial x} - \gamma_w \frac{\partial Z}{\partial x}\right)\right]\Delta x + q_{wsc}\rho_{wsc} m_{cF} + m_{c\_hd} - T_{wMa-F}\,\Delta_{wMa-F}(p_w - \gamma_w Z) = \frac{V_b}{\alpha_c}\frac{\partial}{\partial t}\left(\frac{\phi S_w \rho_{wsc} m_{cF}}{B_w}\right)_{fracture} \qquad \text{..... (3a)}$$

$$T_{Fx} = \beta_c k_x A_x \frac{1}{\mu_w B_w}(\rho_{wsc} m_{cF} k_{rw})_{upstream} \qquad \text{..... (3b)}$$

Ion Transport Equation for the Matrix Domain

$$T_{wMa-F}\left[(p_w - \gamma_w Z)_{fracture} - (p_w - \gamma_w Z)_{matrix}\right] = \frac{V_b}{\alpha_c}\frac{\partial}{\partial t}\left(\frac{\phi S_w \rho_{wsc} m_{cMa}}{B_w}\right)_{matrix} \qquad \text{..... (4a)}$$

$$T_{wMa-F} = \beta_c V_b \sigma \left(\frac{k_{Ma}}{\mu_w B_w}\right)(\rho_{wsc} m_{cMa} k_{rw})_{upstream} \quad \text{..... (4b)}$$

Halite Dissolution Model

Dissolution Model Development: Most kinetic phenomena comprise a sequence of elementary reaction steps; each of which, must surmount a potential energy barrier for the kinetic phenomenon to proceed. The transition state theory (TST) characterizes the rates at which reactants overcome each of these potential energy barriers. In so doing, the theory can be used to determine the reaction rate (Lasaga and Kirkpatrick 1981).

Fig. 2 depicts the potential energy curve for the hydrolysis of NaCl. The TST focuses on the molecular configuration of activated complex (transition state), which is situated at the top of the potential energy barrier.The TST asserts that the forward reaction rate is the product of the concentration of the activated complex and its rate of decomposition. As it relates to mineral dissolution, the TST states that dissolution rates are controlled by desorption kinetics of the activated complex formed on the surface of the reacting mineral (Yadav and Chakrapani 2006).

Using the transition state theory (TST), Aagaard and Helgeson (1982) proposed a method by which ion detachment rate can be quantified. Alkattan, Oelkers et al (1996), using the work of Aagaard and Helgeson (1982), showed that the overall dissolution rate of NaCl from the halite surface (r_c) is given by:

$$r_c = \left(\frac{dm_{Na^+}}{dt}\right) = \left(\frac{dm_{Cl^-}}{dt}\right) = r_+[1 - exp(-A/\sigma RT)] \quad \text{..... (5)}$$

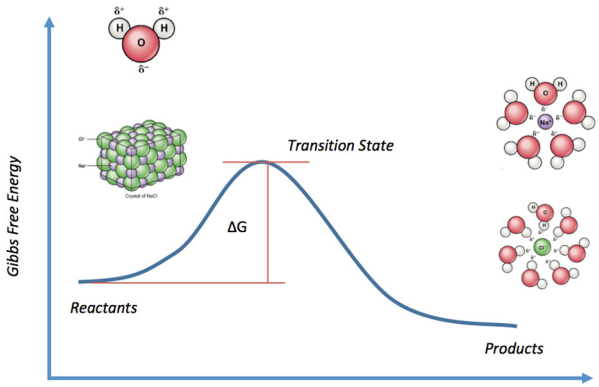

Figure 2: Potential energy curve for the hydrolysis of NaCl (modified from that provided by Openstax College)

This approach efficiently captures the rate at which Na^+ and Cl^- species are detached from the mineral surface, and has therefore been adopted in this work, and coupled with a dual porosity, fully implicit, fluid transport numerical simulator. In this empirical formulation, r_+ is the halite dissolution rate in an infinitely dilute solution, R is the gas constant, T is the absolute temperature, σ is Temkin's average stoichiometric number and $\left(\frac{dm_i}{dt}\right)_{s,c}$ is the flux of the subscripted aqueous species across the mineral fluid interface per unit surface area. A refers to the chemical affinity and is defined as:

$$A = -RT \ln(Q/K) \quad \text{..... (6)}$$

where K is the thermodynamic equilibrium constant for the overall dissolution reaction, and Q is the reaction ionic activity product in solution, which is the product of $a_{Na^+}a_{Cl^-}$. Where a refers to the activity of the subscripted ion.

Combining equations for kinetics and thermodynamics of salt hydrolysis (**Eq. 5** and **Eq. 6,** respectively**)** serves to both incorporate the chemical equilibrium constraints between reactants and activated complex formed in the transition state, and account for the chemical affinity of species on reaction rate (Aagaard and Helgeson 1982).

For the hypothetical reaction:

$$aA + bB \leftrightarrow cC + dD \quad \text{..... (5)}$$

at equilibrium, the equilibrium constant is given by:

$$K = \frac{\{C\}^c\{D\}^d}{\{A\}^a\{B\}^b} \quad \text{..... (6)}$$

where the curly brackets are the thermodynamic activities of the chemical species. Therefore, for the halite dissolution:

$$NaCl \leftrightarrow Na^+ + Cl^- \quad \text{..... (7)}$$

the thermodynamic equilibrium constant, under specified conditions of temperature and pressure, is given by:

$$K = \{Na^+\}\{Cl^-\} \quad \text{..... (8)}$$

since the activity of the solid NaCl species is taken as 1. To estimate activity of ions in solution, measured concentrations of species must be adjusted to account for electrostatic interactions between ions. This is achieved using an ion activity coefficient:

$$a_i = \gamma_i C_i \quad \text{..... (9)}$$

where a_i is the activity and C_i the concentration of species i, and γ_i is the activity coefficient. Activity coefficients are typically calculated by the Extended Debye-Huckel equation, Guntelberg approximation, or Davies equation. However, these empirical formulations are only valid for solutions with ionic strengths $\leq 0.1M$, in the case of the Extended Debye-Huckel equation and Guntelberg approximation, and ≤ 0.5 M in situations where Davies equation is applied. The ionic strength of flowback water, based on the concentration of Na^+ and Cl^- alone, can be expected to be between one and five moles per

liter - well in excess of the range where activity models used in surface and potable groundwater modeling are applicableFor this reason, Pitzer's specific ion interaction (SII) model was employed in this work. The SII model has been used successfully to predict solubilities of highly soluble evaporate minerals in solutions as concentrated as 20M (Drever 1988). According to Pitzer SII model, the activity coefficient (γ_i) for the cation (i) can be calculated from **Eq. 10a** and activity coefficient (γ_j) for the anion (j) can be calculated from **Eq. 10b** (Pitzer 1975; Mesmer and Baes 1976).

$$-log(\gamma_i) = \frac{A(Z_i)^2\sqrt{I}}{1 + Ba_i\sqrt{I}} + \sum_j B_{ij}m_j \quad \text{..... (10a)}$$

$$-log(\gamma_j) = \frac{A(Z_j)^2\sqrt{I}}{1 + Ba_i\sqrt{I}} + \sum_i B_{ij}m_i \quad \text{..... (10b)}$$

A and *B* are Debye-Huckel parameters, both of which are a function of the system temperature and pressure, and a_i is the ion size parameter of the subscripted ion. B_{ij} is the binary specific ion interaction term between ions *i* and *j* and m_j is the molality of the subscripted ion.

One of the challenges with implementing Pitzer's SII model in a numerical reservoir simulator is that the pressure in each numerical grid block changes with time. Even though the reservoir temperature is assumed constant and homogeneous, previously calculated values for *A* and *B* at prescribed temperatures and pressures cannot be utilized. Furthermore, current literature does not provide every value of A and B needed by the simulator during each time step, at the specific reservoir temperature and numerically determined pressure in each grid block. For this reason, the work of Helgeson and Kirkham (1974) was employed to calculate the values of the Debye Huckel parameters (*A* and *B*) at our given reservoir temperature and simulator calculated pressures in each numerical block at each time step. Parameters *A* and *B* are defined as:

$$A \equiv \frac{(2\pi N)^{1/2}e^3\rho^{1/2}}{2.302585(1000)^{1/2}(\varepsilon KT)^{3/2}} \quad \text{..... (11)}$$

$$B \equiv \left(\frac{8\pi N\rho e^2}{1000\varepsilon KT}\right)^{1/2} \quad \text{..... (12)}$$

where N refers to Avogadro's number (6.02252×10^{23} mole^{-1}), e is the absolute electronic charge (4.80289×10^{-10} esu), ρ is density in g/cm^{-3}, ε is the dielectric constant of H_2O, T is the system temperature in Kelvin, and K is Boltzmann's constant (1.38054 × 10-16 erg (°K)$^{-1}$). A has units of Kg^{½} mole$^{-½}$ and B has units of Kg^{½} mole$^{-½}$ cm^{-1} (Helgeson and Kirkham 1974). Malmberg and Maryott (1956) determined the dielectric constant for water(ε) at various temperatures; this work was the source of the dielectric constant used in our simulator.

The final step in the numerical implementation of this model involves the determination of the ion interaction coefficients (B_{ij}). Since B_{ij} is a function of the ionic strength of the solution, and the ionic strength of the solution in each numerical gridblock is different and changes with time, a fixed value for B_{ij} cannot be applied to the numerical simulator. A method is needed to automatically update B_{ij} in each numerical gridblock, across each timestep, as a function of the solution ionic strength. Following the work of Kenneth Pitzer, Baes and Mesmer (1976) showed that the variation of B_{ij} with ionic strength (I) could be represented by the function:

$$B_{ij} = B_{ij}^{\infty} + \left(B_{ij}^{0} - B_{ij}^{\infty}\right).F(I) \quad \text{..... (13)}$$

where

$$F(I) = \frac{1 - \left(1 + 2I^{1/2} - 2I\right)exp\left(-2I^{1/2}\right)}{4I} \quad \text{..... (14)}$$

and

$$F(0) = 1\,; F(\infty) = 0 \quad \text{..... (15)}$$

The coefficients B_{ij}^{0} and B_{ij}^{∞} are the values of B_{ij} at ionic strength of zero and infinity, and *I* is the ionic strength of the solution (Mesmer and Baes 1976). This empirical formulation was incorporated into the numerical simulator to account for the impact that varying ionic strengths, both across time and space, have on the binary specific ion interaction term (B_{ij})

Coupling the halite dissolution model described above, with ion transport model described previously, involves treating the dissolve Na^+ and Cl^- species as an additional source term introduced into **Eq. 3a**.

Salt Module Validation: Numerical models are typically validated internally using a mass balance check, and/or validated externally using the inputs and outputs from similar published models. One of the challenges encountered with this research was to locate other published work that could be used to externally validate the model. Our extensive literature review showed that there was only one other manuscript published that attempted to use a newly developed numerical simulator to predict the ionic composition of flow back water. This work was presented by Gdanski, Weaver et al in 2007. Though an interesting article, sufficient information was not provided on the simulated model or reservoir fluid properties simulated, to allow the results to be used as a means of validating either model. Additionally, there are some fundamental differences between both models that do not allow for simple comparison. The model presented in this manuscript focuses on shale gas formation, specifically Marcellus Shale. It is a 3-Dimentional, dual porosity, fully implicit model that not only captures the effect that mixing

between the injected fluid and formation brine has on flowback water composition, but also captures the potential impact of halite dissolution on this composition. Simulating flow in a hydraulically fractured Marcellus shale well requires that the fracture network, not a single by-wing fracture, is captured in the numerical simulator. The model presented in this manuscript captures the 1ft × 2ft reinitiated natural fracture network seen in Marcellus shale. The model presented by Gdanski and Weaver focuses on tight gas formations and rightly so captures the impact of a single bi-wing fracture (1/2 bi-wing fracture simulated), the model is based on the single porosity concept, it is 2-dimensional, and the source of additional ions added to the flowwack water is solely from concentrated insitu brine. This work was intended to determine the fraction of recovered water that was actually injected fluid and that which was insitu formation brine. This was achieved through composition comparisons among the 3 water types: (1) injected fluid, (2) formation brine. and (3) flow back water.

Given our works novelty, the model was validated internally using a mass balance check (MBC) detailed in Eq. 16, where *m* is the time step number. Definitions for the other terms are found in the manuscript nomenclature. However, the fact that one of the objectives of this work is to compare simulated Na^+ and Cl^- concentrations with actual laboratory measured concentrations of Na^+ and Cl^- seen in Marcellus Shale flowback water is, in and of itself, a field scale external model validation process. If the model is capable of predicting the laboratory measured concentration correctly, it is essentially validated externally.

The input parameters used to validate the model are presented in Table 1; the predicted flowback water ionic composition is presented in Fig. 3 and the mass balance checks are presented in Fig. 4. Results show that the mass balance checks are well within the region of 1.0000000001 and 0.9999999999; this shows that mass is conserved across each time step, and the model is functioning correctly. Further details on the coupled model validation process can be found in other works by the authors (Seales, Wang et al 2015; Seales, Dilmore et al 2015).

Simulation Parameters	Parameter Value
System size	3 x 3 x 3
Block size (x, y , z)	50 ft.
Fracture Spacing	5ft x 5ft
Initial Reservoir Pressure (p_i)	4000 psi
Sandface pressure (psf)	1000 psi
Initial Water Saturation	0.4
k_x, K_y & K_z (Fracture/Matrix)	100 mD / 0.0001mD
Matrix Porosity	10%
Injection (0.5 M - KCl)	168,000 gallons
Insitu Cl^- concentration	50,000 mg/L
Insitu Na^+ concentration	25,000 mg/L
Insitu K^+ concentration	0 mg/L
Well Radius (rw)	0.25 ft.
Well Skin factor (S)	0

Table 1: Model validation parameters

$$MBC = \left[\frac{\sum_{k=1}^{N_z}\sum_{j=1}^{N_y}\sum_{i=1}^{N_x}\left[\left(\frac{V_b\phi S_{w\rho_{wsc}m_{cMa}}}{\alpha_c B_w}\right)_{Ma\,\&\,F}^{t=0} - \left(\frac{V_b\phi S_w\rho_{wsc}m_{cMa}}{\alpha_c B_w}\right)^{n+1}\right]}{\sum_{l=1}^{m}\sum_{k=1}^{N_z}\sum_{j=1}^{N_y}\sum_{i=1}^{N_x}(\rho_{wsc}m_{cF}q_{wsc})^{n+1}\,\Delta t_l^m}\right] \quad (16)$$

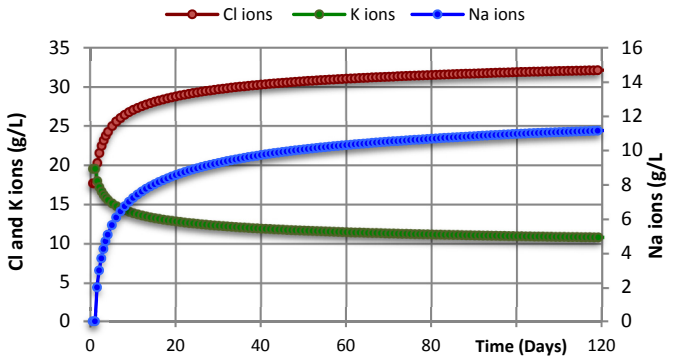

Figure 3: Validation results – Predicted composition

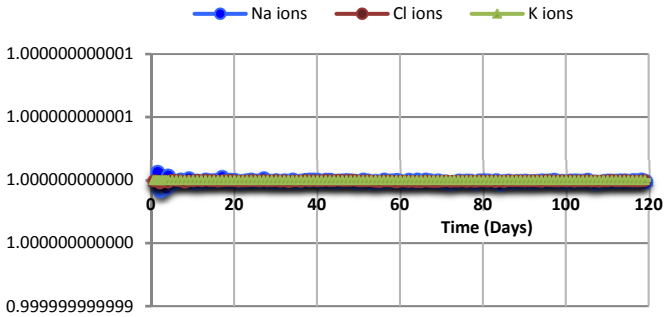

Figure 4: Validation results – Mass balance check

Reservoir Model

The simulated reservoir was based on a traditional shale gas pad layout; six (6) laterals, each approximately one (1) mile long, feed gas to a single well pad (**Fig. 5a**). Our model focused on capturing the stimulated area for a single lateral only (**Fig. 5a**). Using symmetry, one half of the area depleted was modeled (**Fig. 5b**). The numerical grid blocks were then sized using logarithmic grid refinement in both the x and y directions as depicted in **Fig 6.**

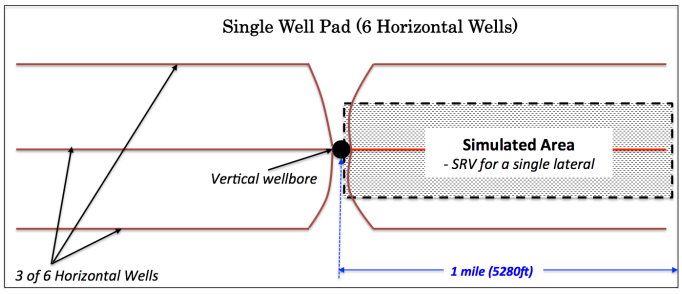

Figure 5a: Stimulated area for a single well pad (5280ft x 2640ft)

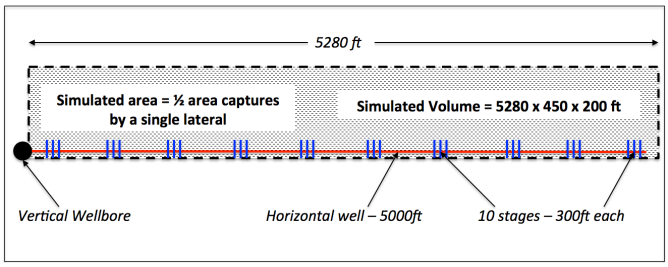

Figure 5b: Illustration of the simulated reservoir layout

We assumed a preexisting fracture network, which was created from a ten (10) stage hydraulic fracturing process; each stage is 300ft in length and has three (3) completion clusters that are evenly spaced (**Fig. 5b**). Fluid injection for hydraulic fracturing, was simulated by injecting 220,000 gallons of a 2% KCL pad fluid into each stage. The spacing of the natural fractures in the stimulated reservoir volume (SRV) was assumed to follow Marcellus J1 and J2 fractures, which are on average 1ft and 2ft apart respectively (**Fig. 6b**) (Engelder, Lash, et al, 2009). Other Relevant simulation parameters are presented in **Table 2**.

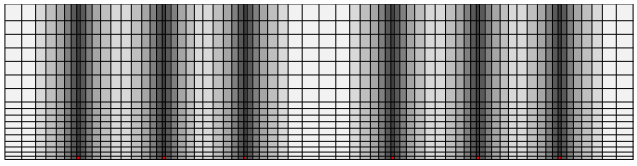

Figure 6a: Numerical blocks grid (Only 2 stages shown for clarity)

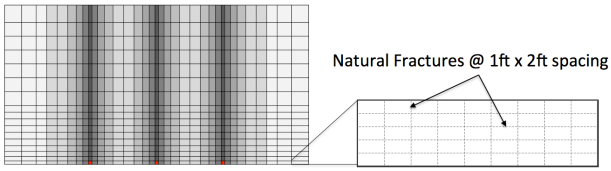

Figure 6b: Natural fracture spacing

Simulation Parameters	Parameter Value
System size (ft)	5280 x 450
Reservoir thickness (ft)	200
Initial pressure (psi)	3500
Sandface pressure (psi)	1000
Initial gas saturation (%)	90
Matrix Permeabiilty	0.0001 mD
Hydraulic fracture conductivity (md-ft)	420
Matrix Porosity	3%
Completion clusters per stage	3
No. of stages	10
Injected Fluid	2% KCl
Fracture fluid per stage (gallons)	220,000
Insitu Cl^- ions	200,000 mg/L
Insitu Na^+ ions	129,692 mg/L
Insitu K^+ ions	0 mg/L
Skin factor	0
Well radius (ft)	0.25

Table 2: Model Simulation parameters

Results and Discussion

Field Case - Composition as a function of mixing only. To explore the source of the excess TDS in flowback water, a first set of simulations was performed to assess the impact that mixing alone, between the injected fracture fluid and in situ formation brine, has on the final ionic composition of flowback water. The simulation parameters are outlined in **Table 2** and the reservoir model is described in **Fig. 5** and **Fig. 6**.

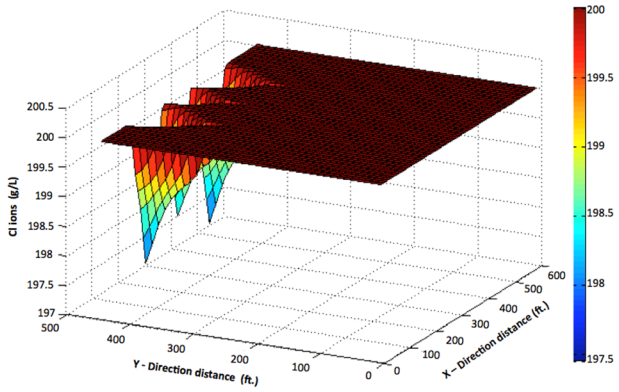

Figure 7a: Simulated Cl^- concentration in the matrix domain after injecting for 1.5 hours (1 fracture stage shown, with 3 completion clusters along the x-axis)

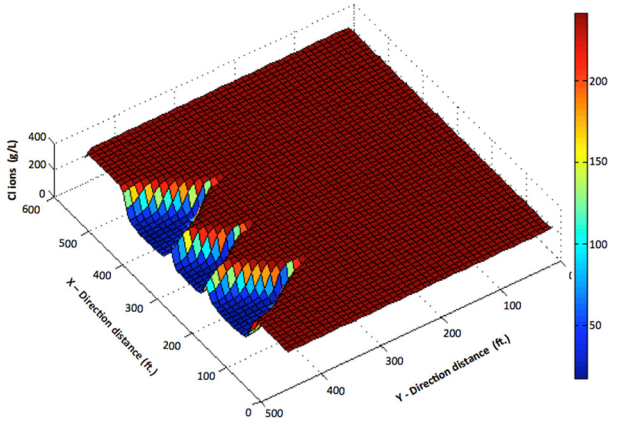

Figure 7b: Simulated Cl^- concentration in the fracture domain after injecting for 1.5 hours (1 fracture stage shown, with 3 completion clusters along the x-axis)

The reservoir was flowed for 1 year and the ion transport module was used to simulate the concentration of Na^+, Cl^- and K^+ species in flowback water, and changes in concentration for each of these species, in both the matrix and fracture domain of each numerical block. Simulated concentration profiles for the Cl^- species, after 20,000 gallon/stage (75,700 liters) of 2 wt % KCl was injected, is presented in **Fig. 7a** and **Fig. 7b**. For clarity, only one stage, which has three (3) perforation clusters, is shown in these figures. Similar profiles are generated for Na^+ and K^+ species. The model simulated flowback water ionic composition is presented in **Fig 8**. Fig. 7a and Fig. 7b show a

reduction in the Cl^- concentration in both the matrix and fracture domains as the injected KCl solution penetrates the formation. A reduction in Cl^- concentrations in the matrix and fracture domain is expected since a more dilute solution (2 wt % KCl) is being injected into a formation that contains insitu brine that is comprised solely of Na^+ and Cl^-. The same observation was made for Na^+ species concentration. However, in the case of the K^+ species in the formation, we observed an expected consistent increase in K^+ concentration as the KCl injection progressed. These results are presented in the Appendix as **Fig. A1** and **Fig. A2**.

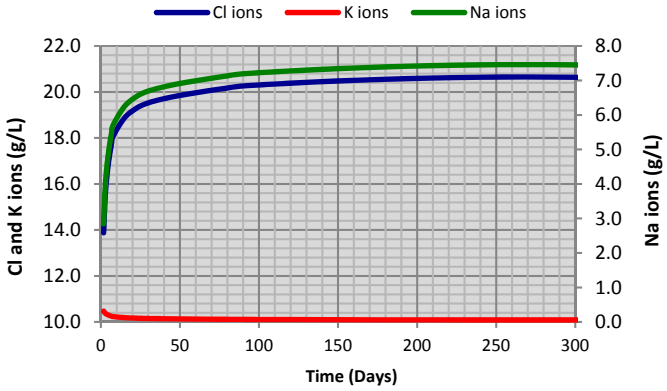

Figure 8: Simulated flowback water ionic composition

Fig. 8 shows that both Na^+ and Cl^- concentration increases rapidly within the first 20 days, then gradually levels off. The shape of the plots can be attributed to the rapid movement of fracture fluid that has mixed with formation brine deep in the formation. This mixture brings extra dissolve salts to the wellbore within the first 20 days of production. Following this period, fluid recovery begins to slow as increasing capillary pressure forces cause the injected fluid to imbibe from the fractures into the rock matrix. The result of this transition is a gradual reduction in volume of salt laden fluids that move from deep in the formation to the wellbore. Consequently, as the drawdown pressure loose ground to capillary pressure and imbibition (between the 20^{th} and 200^{th} day), a gradual decline in fluid recovery accompanied by a gradual decline in both the Na^+ and Cl^- concentration, is obseved. Following the 200^{th} day, the flow of salt laden injected fluid from deep in the formation to the wellbore becomes negligible, along with the impact that this water has on the final flowback water ionic concentrations.

Chemical analysis performed on flowback water from several wells in Marcellus shale shows that after 90 days of production, the Na^+ species concentration in flowback water is in the range of 30 g/L to 120 g/L, and the concentration for Cl^- species fall within the range of 70 g/L to 200 g/L (Hayes 2009). The simulator predicted a maximum 20.64 g/L of Cl^- and just over 7.5 g/L of Na^+ in the flowback water, which resulted from mixing between the injected fluid and in situ formation brine; predicted values are substantially less that those observed in the field. These results suggest two possibilities: (1) the assumed formation brine concentration was too low, or (2) there are other mechanism contributing to the increase in Na^+ and Cl^- species concentration seen in flowback water.

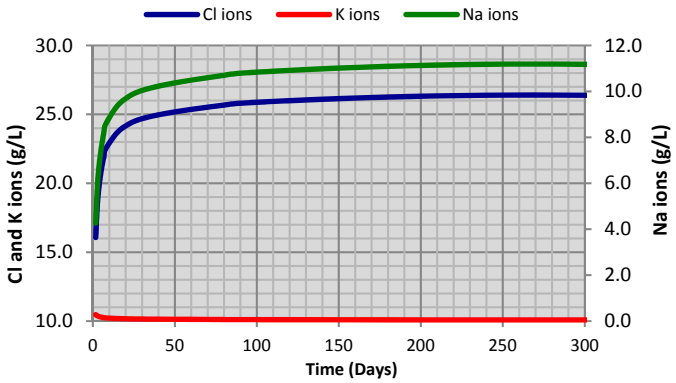

Figure 9: Simulated flowback water ionic composition

Working on the premise that the assumed in situ formation brine concentration was too low, a second simulation was conducted in which the pad fluid composition and volume was held constant (220,000 gallons (833,000 liters) of 2 wt % KCl per stage) but the formation brine ionic concentration was increased by a factor of 1.5. Therefore, in situ Cl^- species concentration was increased to 300 g/L and Na^+ species was increased to 194.5 g/L. Results from this simulation, presented in **Fig. 9,** show that increasing the in situ brine ion concentration by a factor of 1.5 increases the maximum Cl^- and Na^+ species concentration in flowback water to 26.3 g/L and 11.18 g/L respectively. These values are still substantially less that those observed in the field.

1ft x 2ft Simulation Case. It was hypothesize that if the size of the numerical grid blocks was too large, the simulated saturation distribution will not be sufficiently refined to correctly capture mixing between the injected fluid and formation brine. To address this concern, a series of simulations were conducted using a 1ft x 2ft matrix block surrounded by a natural fracture (**Fig. 10**). This arrangement was purposely designed to capture the 1ft x 2ft natural fracture spacing in Marcellus shale. As illustrated in **Fig. 11,** the matrix block was subdivided into numerical blocks ranging in size from ¼ inch to 2 inches. Simulator input parameters are presented in **Table 3**.

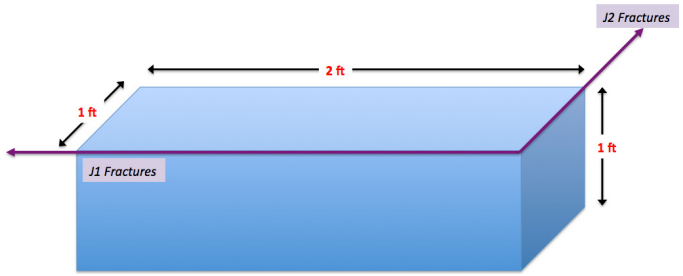

Figure 10: 3D View of simulated reservoir block

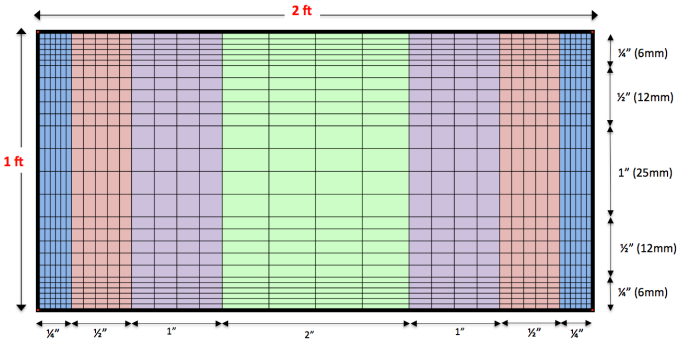

Figure 11: Numerical matrix block gridding

Simulation Parameters	Parameter Value
System size	1ft x 2ft x 1ft
Block size (x,y,z)	varies
Initial pressure	4000 psi
Sandface pressure	500 psi
Matrix initial water saturation $(S_{wi})_{Ma}$	10%
Fracture Initial water saturation $(S_{wi})_F$	99%
Injected Fluid	2% KCl
Injected Volume	0.02 cu.ft
Matrix Porosity	5%
Initial Water Saturation (Swi)	0.3
Matrix Permeabiilty	0.001 mD
Fracture Conductivity	420 md-ft
Insitu Cl^- ions	200,000 mg/L
Insitu Na^+ ions	129,692 mg/L
Insitu K^+ ions	0 mg/L

Table 3: Simulator input parameters

Using the above model, seven simulations were conducted to assess dissolved species concentration in flowback water by changing matrix absolute permeability, matrix capillary pressure, and liquid phase relative permeability (**Fig. 12** and **Fig 13**). Each of these changes was designed to change the volume of mixed fluid recovered, and thus increase the simulated ionic concentration in flowback water. Results for Cl^- and Na^+ species are presented in **Fig. 14** and **Fig. 15**; similar results were obtained for K^+.

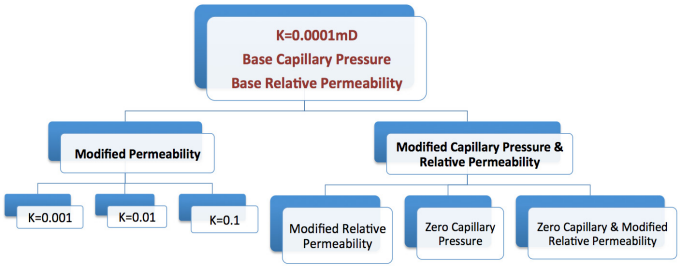

Figure 12: Details of sensitivity analyis performed on simulator inputs

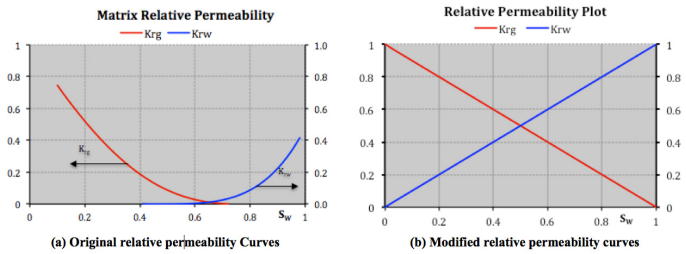

Figure 13: Change made to the relative permeability plots

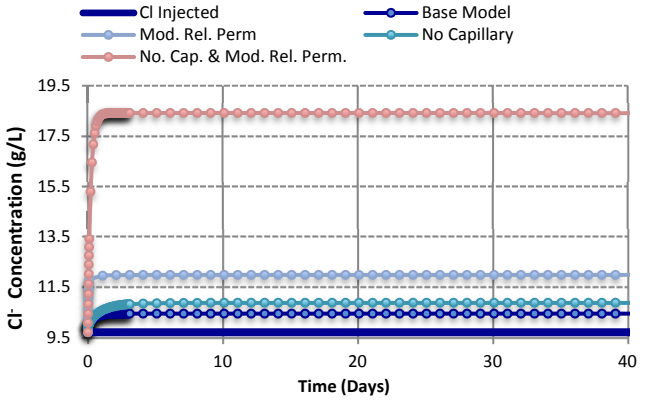

Figure 14: Simulated Cl- species concentration in flowback water

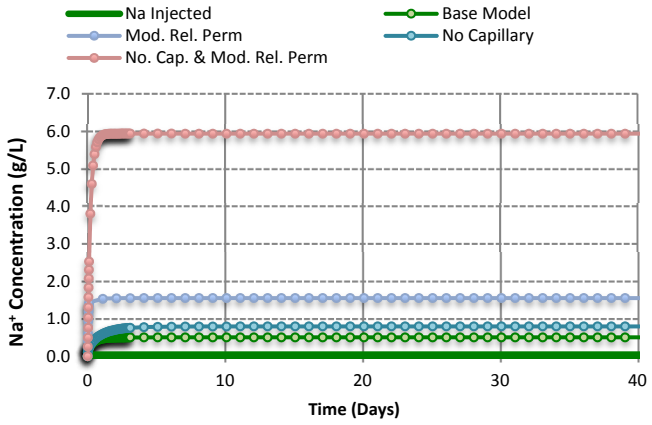

Figure 15: Simulated Na^+ species concentration in flowback water

As a function of mixing between the injected fluid and formation brine, the results show that, no matter the scenario considered, and no matter how unrealistic it is (i.e. no capillary pressure in matrix of a shale formation), it is not possible to obtain Cl^- or Na^+ species concentration similar to those seen in flowback water in the field. The results also show that under the best circumstances, the maximum Cl^- and Na^+ species concentrations attainable in flowback water, as a function of mixing between the injected fluid and formation brine, is 18.4 g/L and 5.95 g/L respectively (Refer to **Fig 14** and **Fig. 15**).

In regards to the simulations that modified the shale matrix absolute permeability, results suggest that increasing the absolute permeability, but maintaining the same matrix

capillary pressure profile, reduces the volume of injected fluid recovered, and reduces the maximum concentration of each species seen in flowback water. If the shale matrix capillary pressure profile is held constant (as was the case in these simulation), such a result is plausible when one considers that increasing the matrix absolute permeability not only improves the rate at which injected fluid and formation water flows back to the fractures, but also improves the rate at which this water imbibes into the rock matrix. Therefore, increasing the absolute permeability (which is typically accompanied by an increase in porosity and a decrease in capillary pressure under naturally occurring conditions) without reducing the capillary pressure forces will typically result in a faster rate of imbibition. This effect is demonstrated in **Figures 16 to 19**, which shows the change in the depth of fluid imbibition along the centerline X-X, as a function absolute permeability and time. These figures show that the depth of fluid imbibition is directly proportional to the matrix absolute permeability at constant capillary pressure.

The results described to this point suggest that mixing between the injected fluid and in situ formation brine is unlikely the only mechanism that causes the high TDS seen in flowback water at the wellhead. High capillary end forces, manifested as high rates of imbibition, limit the amount of in situ brine that is recovered with flowback water, and therefore limit the dissolved species concentrations seen at the wellhead. i.e. shale matrix capillary pressure drives imbibition and prevents recovery of the concentrated "*mixed*" in situ brine. This hypothesis is supported by saturation profiles taken at various times along a bisection line of the simulated reservoir block depicted in **Fig. 20**.

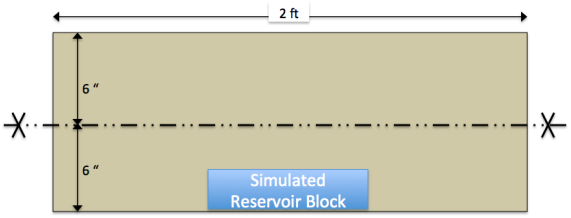

Figure 16: X-X centerline for S_w profiles in Figures 15 to 18

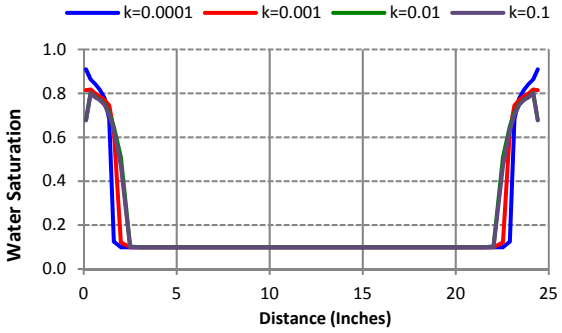

Figure 17: Water saturation profiles along X-X center line after flooding (as a function of matrix absolute permeability)

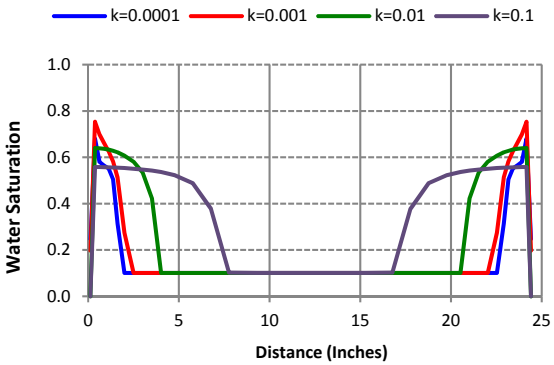

Figure 18: Water saturation profiles along X-X center line after 3 days flowback (as a function of matrix absolute permeability)

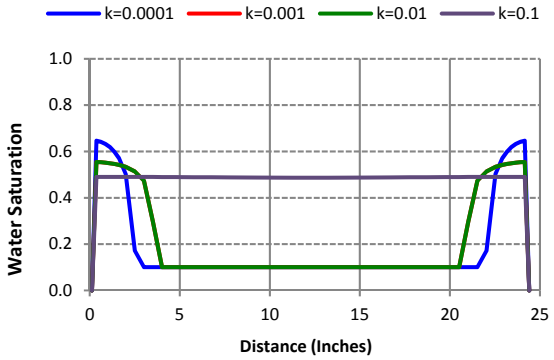

Figure 19: Water saturation profiles along X-X center line after 90 days flowback (as a function of matrix absolute permeability)

Matrix saturation profiles taken at various times along the bisection line of the simulated block (**Fig. 20**), and presented in **Fig. 21**, show: (1) even with high drawdown forces, imbibition continues throughout the entire flowback period, and (2) water saturation within the simulated block quickly climbs from 10% at the end of flooding, to over 50% after 90 days of flowback. Consequently, the majority of the mixed injected fluid that is laden with dissolved ions is not recovered at the wellhead but is transported deeper into the matrix by imbibition. These results further reinforce the hypothesis that other mechanisms, besides mixing between in situ brine and injected fluids, are responsible for the substantial increase flowback water TDS observed at the wellhead.

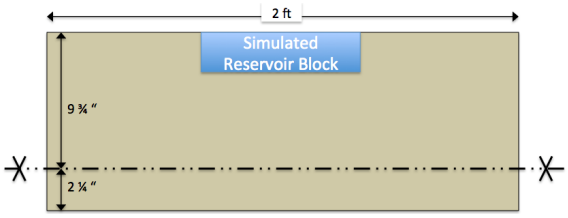

Figure 20: Cross section for water saturation profiles

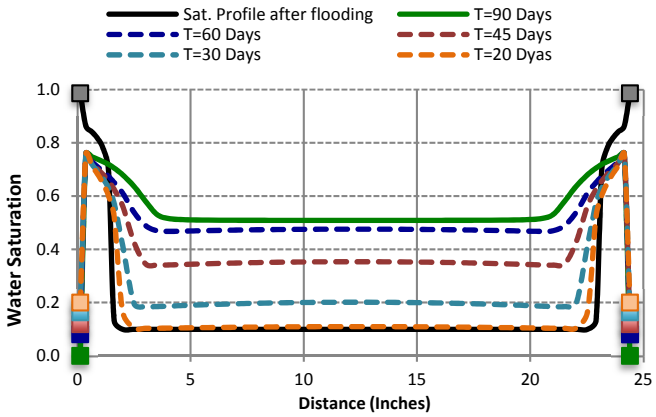

Figure 21: Water saturation along the X-X plane vs. Time

Field Case – Halite Dissolution. Our results showed that the high concentration of Na^+ and Cl^- species in flowback water from hydraulically fractured shale formations is unlikely the results of mixing between the injected fluid and concentrated formation brine. This being the case, simple deduction suggests that there is an additional source of both Na^+ and Cl^- that drives flowback water TDS beyond 150,000 mg/L. The most likely source of these excessive amounts of Na^+ and Cl^- species is Halite. The simulation results presented in this section capture both mixing between the injected fracture fluid and concentrated formation brine, and halite dissolution within the reservoir.

One of the primary inputs to the model is the equilibrium concentration for both Na^+ and Cl^- ions at a given temperature; the concentrations are then converted to activities by the module and used in the dissolution rate calculation. Marcellus shale has a temperature range of 100 °F to 150 °F. The shale formation simulated in this section assumed an average temperature of 130 °F; the solubility of halite at this temperature is 37g/100g H_2O. Converted to molarity, the solubility of halite at 130 °F is 6.217 mol/L (363.347 g/L). This halite solubility equilibrium corresponds to 142.931 g/L of Na^+ and 220.416 g/L of Cl^-, which are used in the model to generate the results in this section.

Under accepted laws of reactive kinetics that govern the dissolution process, the maximum mass of a salt that will dissolve in a pure solvent at a given temperature and pressure is constant, and only changes if one of the following parameters change: (1) Temperature, (2) Pressure, (3) pH, and (4) Solvent purity (i.e., whether the solvent contains other soluble ions). Using halite dissolution in pure water as an example; the mass of both Na^+ and Cl^- species in the solvent will approach, and eventually settle at the dissolution equilibrium mass constant for each ion (142.931 g/L of Na^+ and 220.416 g/L of Cl^- at 130 °F). Halite dissolution in the reservoir was simulated using these equilibrium values and the following assumptions:

1. Reservoir temperature is 130 °F
2. Same temperature exist through the entire reservoir volume
3. Neutral pH
4. Temperature is constant with time
5. There is no preferential detachment of Na^+ or Cl^- species from the halite mass.
6. Other dissolve ions in the injected fluid and in situ formation water have a negligible effect on halite dissolution rate and equilibrium state.
7. Other reactions in the formation, besides halite dissolution, have a negligible impact on the Na^+ and Cl^- species concentration in the flowback water.

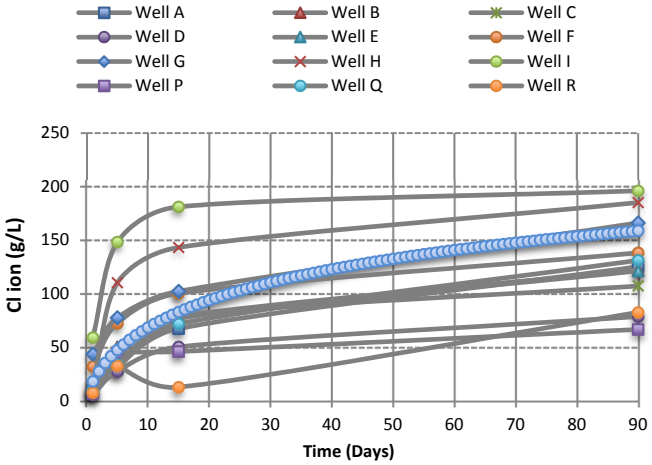

Figure 22: Simulated Cl^- concentration in flowback water

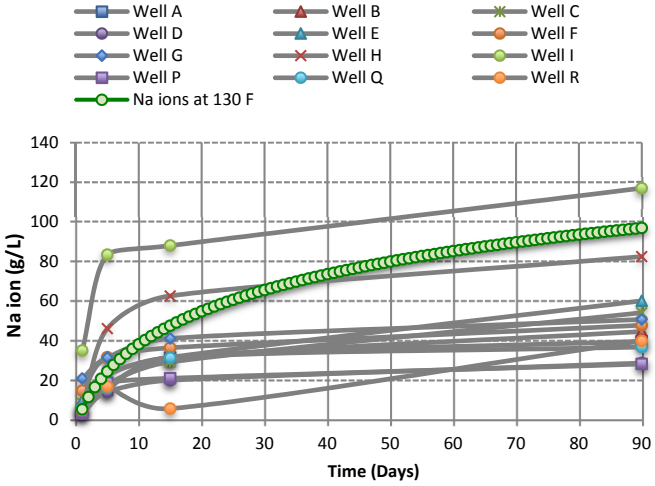

Figure 23: Simulated Na^+ concentration in flowback water

Using these assumptions and the same simulation parameters outlined in **Fig. 5** to **Fig. 6** and **Table 2**, simulated Na^+ and Cl^- species concentration in flowback water is presented in **Fig. 22** and **Fig. 23** above, along with concentration profiles generated from chemical analysis performed on flowback water from 12

Marcellus shale wells (Hayes 2009). Halite dissolution at far from equilibrium conditions (r_+) at 25 °C was taken as 0.616595 $molm^{-2}s^{-1}$ (Palandri and Kharaka 2004). Since the reservoir is at 130 °F (54.44 °C), Arrhenius equation was used to adjust the halite dissolution rate to 0.806354 mol/m s. The predicted halite dissolution rates are presented in **Fig. 24**.

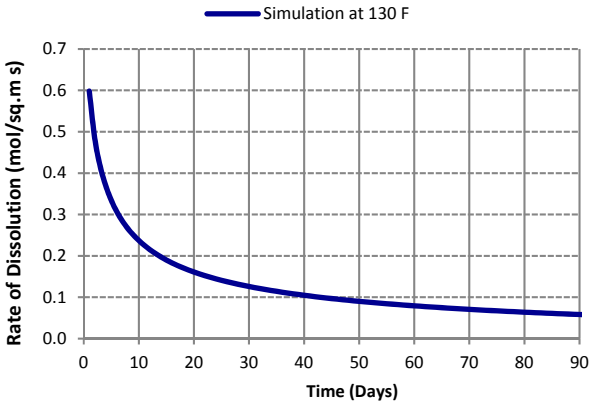

Figure 24: Simulated halite dissolution rate at 130 °F

The inclusion of halite dissolution increases the maximum concentration of Cl^- ions seen in flowback water from 20.64 g/L (if mixing alone is captured) to 158 g/L. Maximum Na^+ concentration in flowback water increased from 7.5 g/L (if mixing alone is assumed) to 96 g/L after halite dissolution is captured. Unlike previously simulated concentrations, which were based on mixing only, these new results fall within the range of Cl^- and Na^+ concentrations seen in flowback water in the field. However, a comparison of the simulated data with field data shows that the simulated concentration for both Na^+ and Cl^-, at a reservoir temperature of 130 °F, falls within the higher range of the field data presented on the same plots. One plausible reason is that the field data was from reservoirs with temperatures that are much less than 130 °F. To test the effect that temperature has on the final flowback water composition, a second simulation was conducted using the same input parameters but assuming a 100 °F reservoir temperature. These results are presented in **Fig. 25** to **Fig. 27**.

Changing the water temperature by 30 °F does not significantly change halite solubility (**Table 4**). However, the far from equilibrium dissolution rate for halite decreased from 0.8063 to 0.6970 mol/m s or -13%. Results from these simulations show that a 30 °F change in the reservoir temperature has only a marginal impact on the simulated flowback water Na^+ and Cl^- concentrations. The impact of the temperature change is most prominent in the early time flowback period but quickly dissipates as flowback surpasses two (2) weeks (refer to **Fig. 27**). This observation can be attributed to smaller volumes of water available for flowback during the later time. Therefore, a 13% reduction in the halite dissolution rate will not substantially change the ionic content of this small volume of water so much that the change is easily visible at the well head.

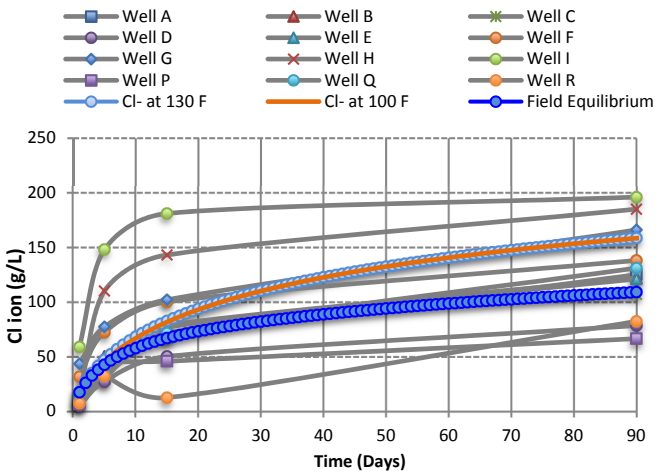

Figure 25: Simulated Cl^- concentration in flowback water at T=100 °F

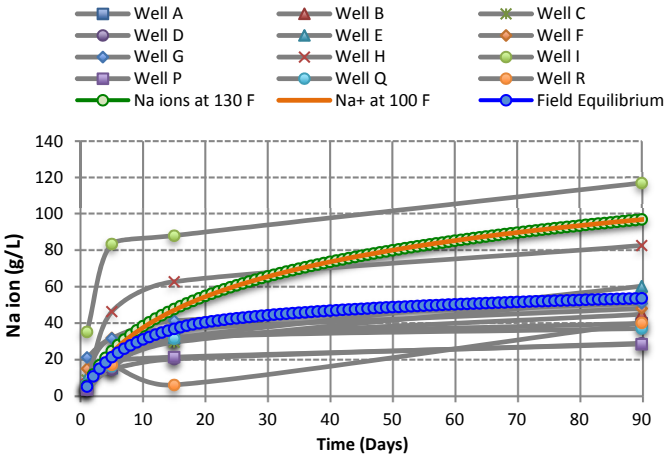

Figure 26: Simulated Na^+ concentration in flowback water at T=100 °F

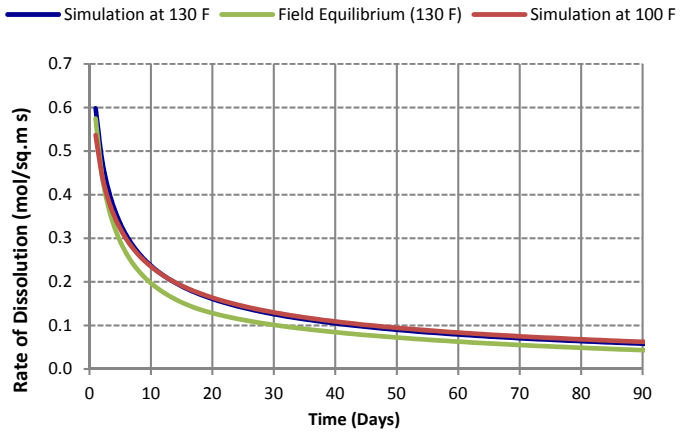

Figure 27: Simulated halite dissolution rate at T=100 °F and T=130 °F

Temperature	Halite Solubility g/100g H_2O	Equilibrium Cl^- (g/L)	Equilibrium Na^+ (g/L)	Far from Equilibrim Dissolution Rate mol m^{-2} s^{-1}
130 °F	37.00	220.42	142.93	0.8063
100 °F	36.31	217.63	141.13	0.6970

Table 4: Simulation reactive kinetics parameters

Simulated vs. Reported Concentrations. Although the simulated Cl^- concentration in flowback water for reservoirs at 100 ºF and 130 ºF fall within the range of concentrations measured in the field, the Na^+ concentration predicted in both these cases are in the higher range of field values. Interestingly, a molar balance on the Na^+ and Cl^- present in flowback water after 90 days, for each of the 12 wells tested, shows that the Na^+ ion concentration is substantially less than that for a balance Na-Cl system; these results are summarized in **Table 5**.

Two assumptions made in the halite dissolution simulations are: (1) other dissolve ions (besides Na^+& Cl^-) in the injected fluid and formation water have a negligible effect on halite dissolution rate and, (2) other reactions in the formation, besides halite dissolution, have a negligible impact on both Na^+ and Cl^- concentration. This means the simulated formation water and injected fluid will be charge balanced with Na^+ and Cl^- ions, and the effects of other reactions (besides halite dissolution), which can change Na^+ and/or Cl^- concentration in the formation water, are negligible. However, under field conditions, this simplifying assumption may not hold true (Chapman, Capo et al 2012; Mohan, Hartsock et al 2013). The consequence of this is slightly higher predicted concentrations for both Na^+ and Cl^- species than those typically seen in the field. Refer to **Fig. 21** and **Fig. 22**.

Description	Measured Cl^- (g/L)	Measured Na^+ (g/L)	Charge Balance Na^+ (g/L)	Na^+ Difference (g/L)
Equilibrium at 130 °F	**220.42**	**142.93**	**142.93**	**0.00**
Approx. well equilibrium	**150**	**60.00**	**97.27**	**37.27**
Well A	125	39.70	81.06	41.36
Well B	122	44.60	79.11	34.51
Well C	107	54.10	69.39	15.29
Well D	78.3	28.7	50.77	22.07
Well E	121	60.1	78.46	18.36
Well F	138	47.8	89.49	41.69
Well G	166	50.7	107.64	56.94
Well H	185	82.5	119.96	37.46
Well I	196	117	127.10	10.10
Well P	66.3	28.2	42.99	14.79
Well Q	131	36.8	84.95	48.15
Well R	82.2	39.9	53.30	13.40

Table 5: Na^+ and Cl^- species concentration in flowback water at 90 days flowback (Source: Hayes 2009)

Referring to **Table 5**, and using well A as an example. The ion concentration profiles for this well, shown in **Fig. 25** and **Fig. 26**, suggest that under field conditions the balanced concentration for Cl^- after 90 days flowback is approximately 125 g/L. The corresponding Na^+ concentration at this point in time for the same well is 39.7 g/L. However, according to our model assumptions, and neglecting the negligible mass of K^+ injected with the 2% KCl solution, a charge balance for this system will require 81.06 g/L of Na^+ ions. This equates to an extra 41.36 g/L of Na^+ than is present in the flowback water in the field at 90 days. This observation suggests that there are other reactions that are either adding additional Cl^- ions to the system (perhaps the dissolution of other salts), or reactions that are removing Na^+ ions from the system (such as precipitation); the latter scenario being most likely. Consequently, when we simulate the preceding scenario, since we are not considering auxiliary reactions that are possibly reducing the Na^+ species concentration, the predicted concentration for Na^+ will be in the vicinity of 81.06 g/L and not 39.7 g/L. However, from a purely theoretical standpoint, one can account for the auxiliary reactions that are impacting the system. This is achieved by constraining the numerical model to an equilibrium condition that has a maximum dissolvable Na^+ and Cl^- species equal to 39.7 g/L and 125 g/L respectively (as measured in the field), instead of 142.93 g/L and 220.42 g/L as calculated by a charge balance on Na^+ and Cl^-.

Having assessed the shape of the concentration profiles measured in the field, and presented in **Fig. 25** and **Fig. 26** for Cl^- and Na^+ respectively; we observed that the Cl^- concentration for the majority of the wells fell below or approach 150 g/L, and the Na^+ concentration for these wells fell below or approach 60 g/L. Assuming that the maximum mass of Cl^- and Na^+ species that can be dissolved by formation water is 150 g/L and 60 g/L respectively, and not 220.42 g/L Cl^- and 142.93 g/L Na^+, as is the case with pure water at 130 ºF (Refer to **Table 5**), flowback was again simulated for 90 days, and flowback water Na^+ and Cl^- species concentrations predicted. The results from this simulation are presented in **Fig. 25** to **Fig. 27** (labeled field equilibrium), and **Table 6**. Having captured to some extent the impact that other formation reactions (besides halite dissolution) have on flowback water Na^+ and Cl^- species concentrations, the simulator results are now a perfect match to those seen in the field. One can therefore conclude that there are auxiliary reactions taking pace in the formation, besides halite dissolution, that substantially impact the final Na^+ and Cl^- species concentration seen in flowback water, and these reactions must be accounted for to ensure simulation accuracy.

Simulation Description	Concentration in Flowback Water (g/L)											
	1 Day		5 Days		15 Days		30 Days		45 Days		90 Days	
	Na^+	Cl^-	Na^+	Cl^-	Na^+	Cl^-	Na^+	Cl^-	Na^+	Cl^-	Na^+	Cl^-
Mixing Only	2.8	13.9	5.2	17.4	6.2	18.9	6.7	19.5	6.9	19.8	7.2	20.3
Mixing and Halite Dissolution	5.2	17.6	24.4	47.0	45.9	80.0	63.7	107.4	78.7	130.6	96.3	157.6
Halite Dissolution Only	2.4	3.7	19.2	29.6	39.7	61.2	57.0	87.9	71.8	110.8	89.1	137.4
Dissolution Contribution (%) - Na^+	45.8		78.6		86.4		89.5		91.2		92.5	
Dissolution Contribution (%) - Cl^-		21.1		63.0		76.4		81.8		84.8		87.1

Table 6: Contribution of halite dissolution to flowback water Na^+ and Cl^- species concentration

Conclusions

In this work, an ion transport and halite dissolution model was coupled with a fully implicit, dual porosity, finite difference numerical simulator. The model starts the process of closing the gap in knowledge as it relates to the accurate prediction of flowback water composition and the identification of the predominant physical and chemical phenomena that are responsible for substantial changes seen in the injected fluid composition during flowback (recovery). With such a model, operators are positioned to better plan for and complete frontend designs for flowback water treatment, reuse and/or disposal. Furthermore, such a model can be used by government agencies, as a management tool, in tracking and predicting the volumes and composition flowback and produced water. Results from this study, and subsequent analysis supports the following conclusions:

1. Mixing alone between the injected fracture fluid and in situ formation brine cannot account for the high concentration of Na^+ (~50 g/L) and Cl^- (~ 120 g/L) species seen in flowback water from fractured shale formations. Mixing accounts for a maximum 20.64 g/L of Cl^- and just over 7.5 g/L of Na^+ in the flowback water.
2. High capillary pressure in the shale formation limits the amount of in situ brine that is recovered with flowback water, and therefore limits the simulated dissolve species concentration (as a function of mixing only) seen in flowback at the wellhead.
3. Increasing the shale matrix absolute permeability, while maintaining the same matrix capillary pressure profile, increases the rate of imbibition, reduces the volume of mixed fluid recovered, and therefore reduces the simulated dissolved species maximum concentration in flowback water.
4. Improving the relative permeability to water in the matrix domain will have a greater impact on the volume of injected fluid recovered than will decreasing the capillary pressure.
5. Halite dissolution is a major contributor to the mass of Na^+ and Cl^- species seen in flowback water. Halite dissolution can account for as much as 81% of Cl^- and 86.5% of Na^+ species seen in 90-day flowback water.
6. Reservoir temperature can affect halite dissolution rate. However, changes in dissolution rate brought on my reservoir temperature changes are not so significant that the impact on Na^+ and Cl^- species concentration is easily visible at the wellhead.

The results suggest that there are other reactions taking place in the formation, besides halite dissolution, that impact the final Na^+ and Cl^- species concentration seen in flowback water at the wellhead from hydraulically fractured shale formations. Future work in this area of study should focus on capturing the most pertinent of these reactions. Additionally, one may also wish to assess the impact that dissolved species diffusion can have on flowback water solute concentration. However, it is our opinion that since the fractures are the main conduits for fluid recovery in fractured shale formation, and considering the velocity of the fluid in these fractures, the impact of diffusion on flowback water species concentration (TDS) will be negligible. For this reason it was not modeled in the foregoing simulations.

Nomenclature

$\mathbf{A}$ - Area, ft^2

$\mathbf{B_w}$ - Water formation Volume factor, RB/STB

$\boldsymbol{k}$ - Absolute permeability, mD

$\boldsymbol{k_r}$ - Relative permeability, mD

$\mathbf{m_c}$ - Component 'c' weight fraction, lbm/lbm

m_{c_hd} - Mass of component 'c' from halite dissolution

$\mathbf{M}$ - Molar mass, g/mol

$\mathbf{N_z, N_y, N_x}$ - Number of grid blocks in the z, y and x directions

$\boldsymbol{P_{cgw}}$ - Capillary pressure (gas and water phase), psi

$\boldsymbol{p}$ - Pressure, psi

$\mathbf{q_w}$ - Water flow rate, STB/D

$\boldsymbol{s}$ - Saturation, fraction

$\boldsymbol{V_b}$ - Bulk volume, ft^3

$\boldsymbol{z}$ - Gas compressibility factor

$\boldsymbol{Z}$ - Elevation referenced from datum, ft

α_c - Volume conversion factor, 5.614583

β_c - Transmissibility conversion factor, 1.127

$\boldsymbol{\rho}$ - Density, lbm/ft^3

$\boldsymbol{\phi}$ - Porosity, fraction

$\boldsymbol{\mu}$ - Viscosity, cp

$\boldsymbol{\gamma_p}$ - Gravity of phase p, psi/ft

Δ - Gradient operator

Subscripts

F - Fracture domain

g - Gas phase

Ma - Matrix domain

Ma_F - Matrix – Fracture domain boundary

sc - Std. conditions

w - Water phase

References

Aagaard, P. and Helgeson, H. (1982). Thermodynamic and kinetic constraints on reaction rates among minerals and aqueous solutions; I, Theoretical considerations. *American journal of Science* **282** (3): 237-285.

Alkattan, M., Oelkers, E. H. et al. (1996). Experimental studies of halite dissolution kinetics, 1 The effect of saturation state and the presence of trace metals. *Chemical Geology* **137** (3): 201-219.

Bazin, B. and J. Labrid (1991). Ion Exchange and Dissolution/ Precipitation Modeling: Application to the Injection of Aqueous Fluids Into a Reservoir Sandstone. *SPE Reservoir Engineering* **6** (2): 233-238.

Bhuyan, D., L. W. Lake, et al. (1990). Mathematical Modeling of High-pH Chemical Flooding. *SPE Reservoir Engineering* **5** (2): 213-220.

Blauch, M., Myers R., et al. (2009). Marcellus Shale Post-Frac Flowback Waters - Where is All the Salt Coming from and What are the Implications?. Presented at the SPE Eastern Regional Meeting, 23-25 September, Charleston, West Virginia, USA. SPE-125740-MS.

Brezonik, P. and Arnold, W. (2011). Water chemistry: an introduction to the chemistry of natural and engineered aquatic systems. Oxford University Press.

Bryant, S. L., R. S. Schechter, et al. (1986). Interactions of precipitation/dissolution waves and ion exchange in flow through permeable media. *AIChE Journal* **32** (5): 751-764.

Chapman, E.C., Capo, R.C., Stewart B.W. (2012). Geochemical and strontium isotope characterization of produced waters from Marcellus shale natural gas extraction. *Environmental Science & Techology* **46** (6): 3545 – 3553

Drever, J. I. (1988). The geochemistry of natural waters. Englewood Cliffs, N.J.: Prentice-Hall.

Engelder, T., Lash, G. and Uzcategui, R. (2009). Joint sets that enhance production from middle and upper devonian gas shales of the appalachian basin. AAPG Bulletin **93** (7): 857-889.

Gdanski, R. D., Weaver, J. et al. (2007). A New Model for Matching Fracturing Fluid Flowback Composition. Presented at the SPE Hydraulic Fracturing Technology Conference, 29-31 January, College Station, Texas, U.S.A. SPE-106040-MS.

Haluszczak, L. O., A. W. Rose, et al. (2013). Geochemical evaluation of flowback brine from Marcellus gas wells in Pennsylvania, USA. *Applied Geochemistry* **28** (0): 55-61.

Hayes, T. (2009). Sampling and Analysis of Water Streams Associated with the Development of Marcellus Shale Gas. G. T. Institute, Marcellus Shale Coalition.

Hayes, T. and B. Severin (2012). Characterization of Flowback Waters from the Marcellus and the Barnett Shale Regions. Barnett and Appalachian Shale Water Management and Reuse Technologies RPSEA.

Helgeson, H. C. and D. H. Kirkham (1974). Theoretical prediction of the thermodynamic behavior of aqueous electrolytes at high pressures and temperatures; II, Debye-Huckel parameters for activity coefficients and relative partial molal properties. *American journal of Science* **274** (10): 1199-1261.

Horn, A. D. (2009). Breakthrough mobile water treatment converts 75% of fracturing flowback fluid to fresh water and lowers CO2 emissions. Presented at SPE Americas E&P Environmental and Safety Conference, 23-25 March, San Antonio, Texas. SPE-121104-MS.

Lasaga, A. C. and R. J. Kirkpatrick (1981). Kinetics of geochemical processes. 3 Vol. 8. Reviews in Mineralogy.

Liu, X. and P. Ortoleva (1996). A General-Purpose, Geochemical Reservoir Simulator. Presented at the SPE Annual Technical Conference and Exhibition, 6-9 October, Denver, Colorado. SPE-36700-MS.

Malmberg, C. and A. Maryott (1956). Dielectric Constant of Water from 00 to 100 C. *Journal of research of the National Bureau of Standards* **56**: 1-8.

Mesmer, R. and C. Baes (1976). The hydrolysis of cations.Wiley.

Mohan, A.M., Hartsock, A., Hammack R.W. et al (2013) Microbial communities in flowback water impoundments from hydraulic fracturing for recovery of shale gas. *FEMS Microbial Ecol* **86** (3):567-580

OpenStax College [CC BY 3.0 (http://creativecommons.org/licenses/by/3.0)], via Wikimedia Commons. http://commons.wikimedia.org/wiki/File%3A214_Dissociation_of_Sodium_Chloride_in_Water-01.jpg

Palandri, J. and Y. K. Kharaka (2004). A Compilation of Rate Parameters of Water-Mineral Interaction Kinetics for Application to Geochemical Modeling. USGS and N ETL, U.S. Geological Survey.

Paugh, L. O. (2008). Marcellus Shale Water Management Challenges in Pennsylvania. Presented at the SPE Shale Gas Production Conference, 16-18 November, Fort Worth, Texas, USA. SPE-119898-MS.

Pitzer, K. S. (1975). Thermodynamics of electrolytes. V. Effects of higher-order electrostatic terms. *Journal of Solution Chemistry* **4** (3): 249-265.

Puder, M. and Veil, J. (2006). Offsite commercial disposal of oil and gas exploration and production waste: availability, options, and cost. ANL.

Seales, M., Wang, J.Y. & Ertekin, T. (2015). Analysis of Fracture Fluid Cleanup and Long-term Recovery in Shale Gas Reservoirs, Dissertation/Thesis, Pennsylvania State University.

Seales, M., Dilmore, R., Ertekin, T., & Wang, J.Y. *In press*. A Numerical Study of Factors Affecting Fracture Fluid Cleanup and Produced Gas/Water in Marcellus Shale (Part II). *SPE Journal.* (submitted 29 November 2015).

Shafer, L. (2011). Water Recycling and Purification in the Pinedale Anticline Field: Results From the Anticline Disposal Project. Presented at the SPE Americas E&P Health, Safety, Security, and Environmental Conference, 21-23 March, Houston, Texas, USA. SPE-141448-MS.

Sparks, D. L. (2003). Environmental soil chemistry. Academic press.

Stepan D. J., Shockey, R., Kurz, B. et al (2010). Bakken Water Opportunities Assessment - Phase 1 Energy and Environmental Research Centre, University of North Dakota.

Stumm, W. and R. Wollast (1990). Coordination chemistry of weathering: Kinetics of the surface□controlled dissolution of oxide minerals. *Reviews of Geophysics* **28** (1): 53-69.

Walter, A. L., E. O. Frind, et al. (1994). Modeling of multicomponent reactive transport in groundwater: 1. Model development and evaluation. *Water Resources Research* **30** (11): 3137-3148.

Yadav, S. K. and Chakrapani, G. (2006). Dissolution kinetics of rock-water interactions and its implications. *Current Science* **90** (8): 932-937.

Yang, L., Grossmann, I. E., and Mauter, M. S. et al (2015). Investment optimization model for freshwater acquisition and wastewater handling in shale gas production. *AIChE Journal.* doi: 10.1002/aic.14804

Zhou, Q., Dilmore, R., Kleit, A. N., & Wang, J. Y. (2015). Evaluating Fracturing Fluid Flowback in Marcellus Using Data Mining Technologies. Presented at the SPE Hydraulic Fracturing Technology Conference, 3-5 February, The Woodlands, Texas, USA. SPE-173364-MS.

Appendix

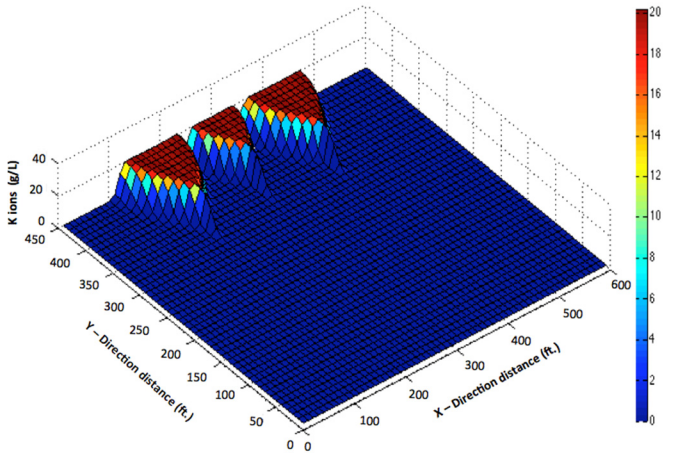

Figure A1: Simulated K^+ concentration in the fracture domain

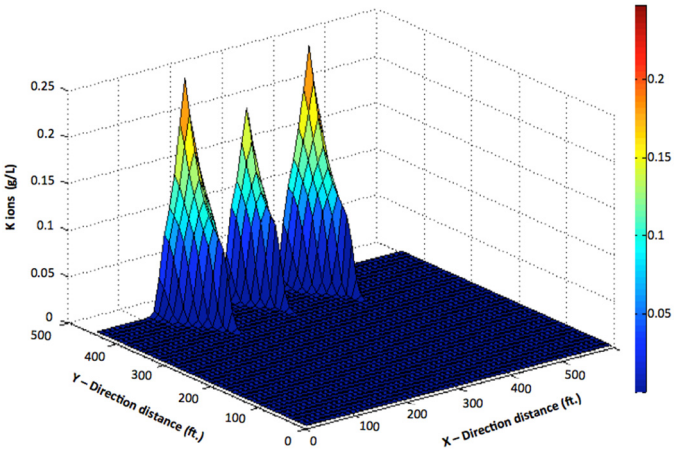

Figure A2: Simulated K^+ concentration in the matrix domain